Supporting Information for

Unique switching mode of HfO_2 among fluorite-type ferroelectric candidates

Ge-Qi Mao,[1,#] Heng Yu,[1,#] Kan-Hao Xue,[1,2,a)] Jinhai Huang,[1] Zijian Zhou,[1] and Xiangshui Miao[1,2]

[1]School of Integrated Circuits, Huazhong University of Science and Technology, Wuhan 430074, China

[2]Hubei Yangtze Memory Laboratories, Wuhan 430205, China

[a)]Author to whom correspondence should be addressed: xkh@hust.edu.cn

[#]These authors contributed equally.

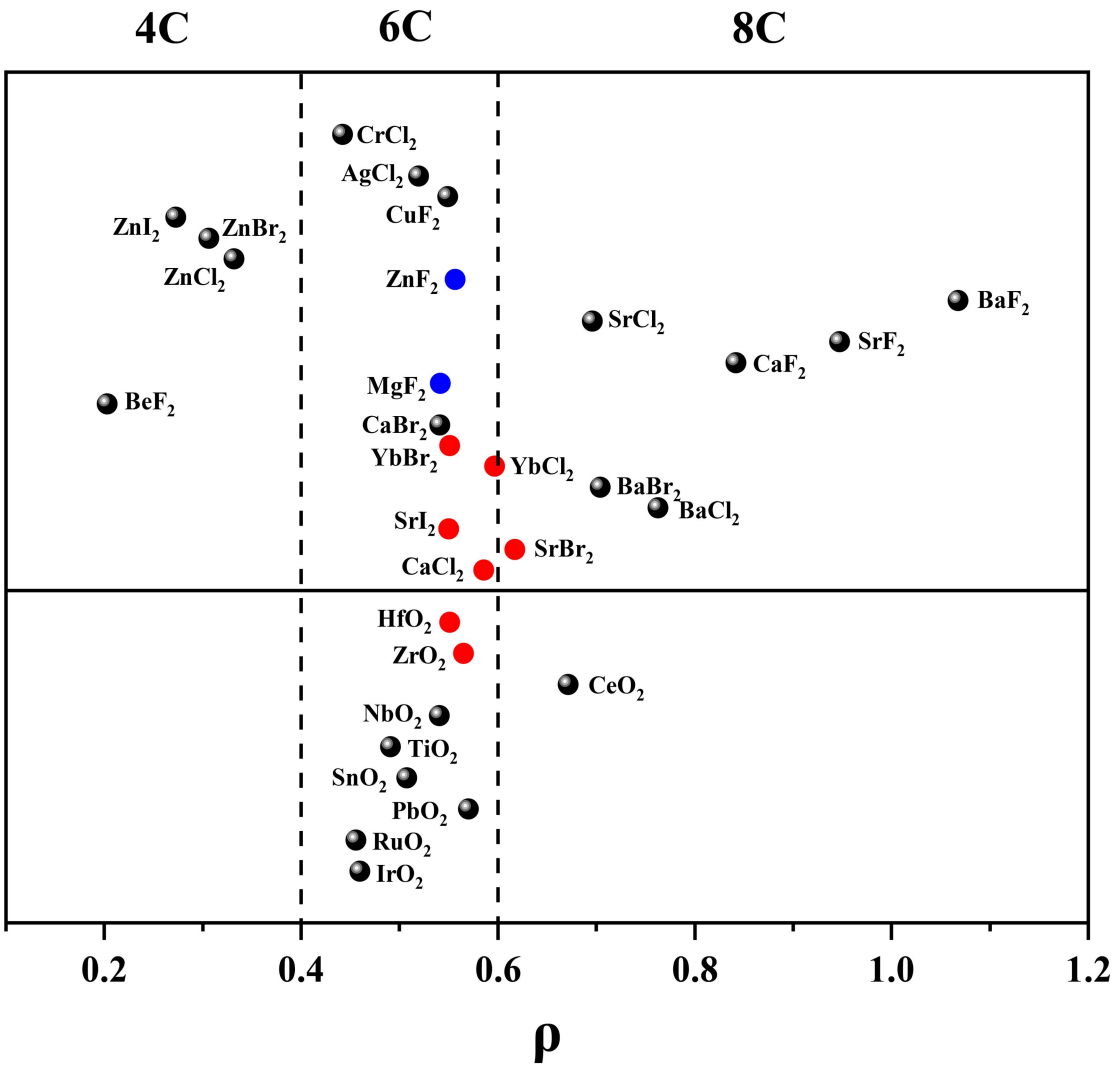

Figure S1： Statistical graph of coordination number and radius ration of common binary materials.

Figure S1 shows the relationship between the cation/anion radius ratio and the coordination number of common binary compounds. It can be seen that ρ=0.6 is the boundary between 6C and 8C. The radius ratio of HfO_2, ZrO_2, SrI_2, $SrBr_2$, $CaCl_2$, $YbCl_2$ and $YbBr_2$ is around 0.6, marked with a red ball. The radius ratio of MgF_2 and ZnF_2 is also around 0.6, marked with a blue ball. However, these two materials cannot maintain limited spontaneous polarization under the *Pca*2_1 phase via our calculations, so MgF_2 and ZnF_2 are not discussed in manuscript.

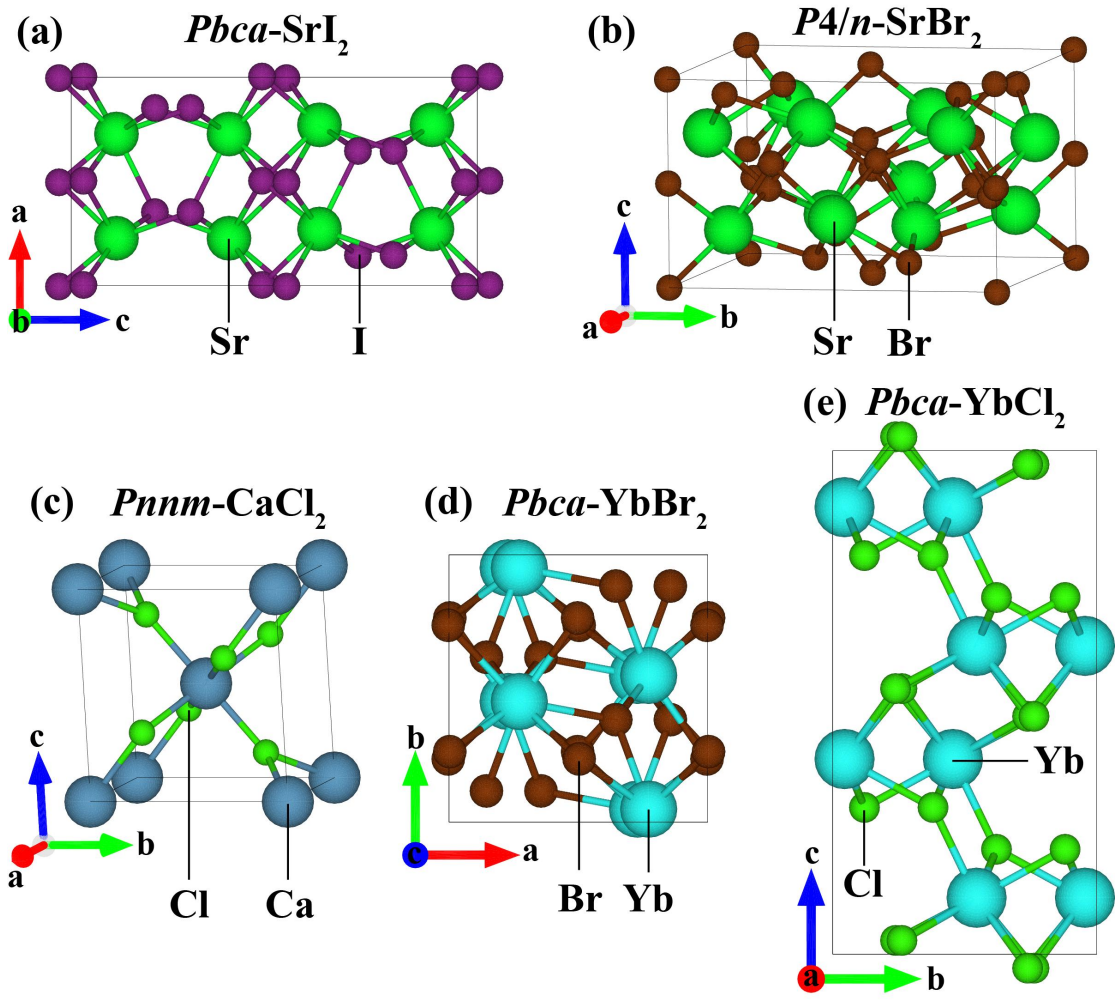

Figure S2. The schematic diagrams of the ground-state structures for the five materials, where (a), (d), and (e) represent illustrations of the *Pbca* structure viewed along three different orientations.

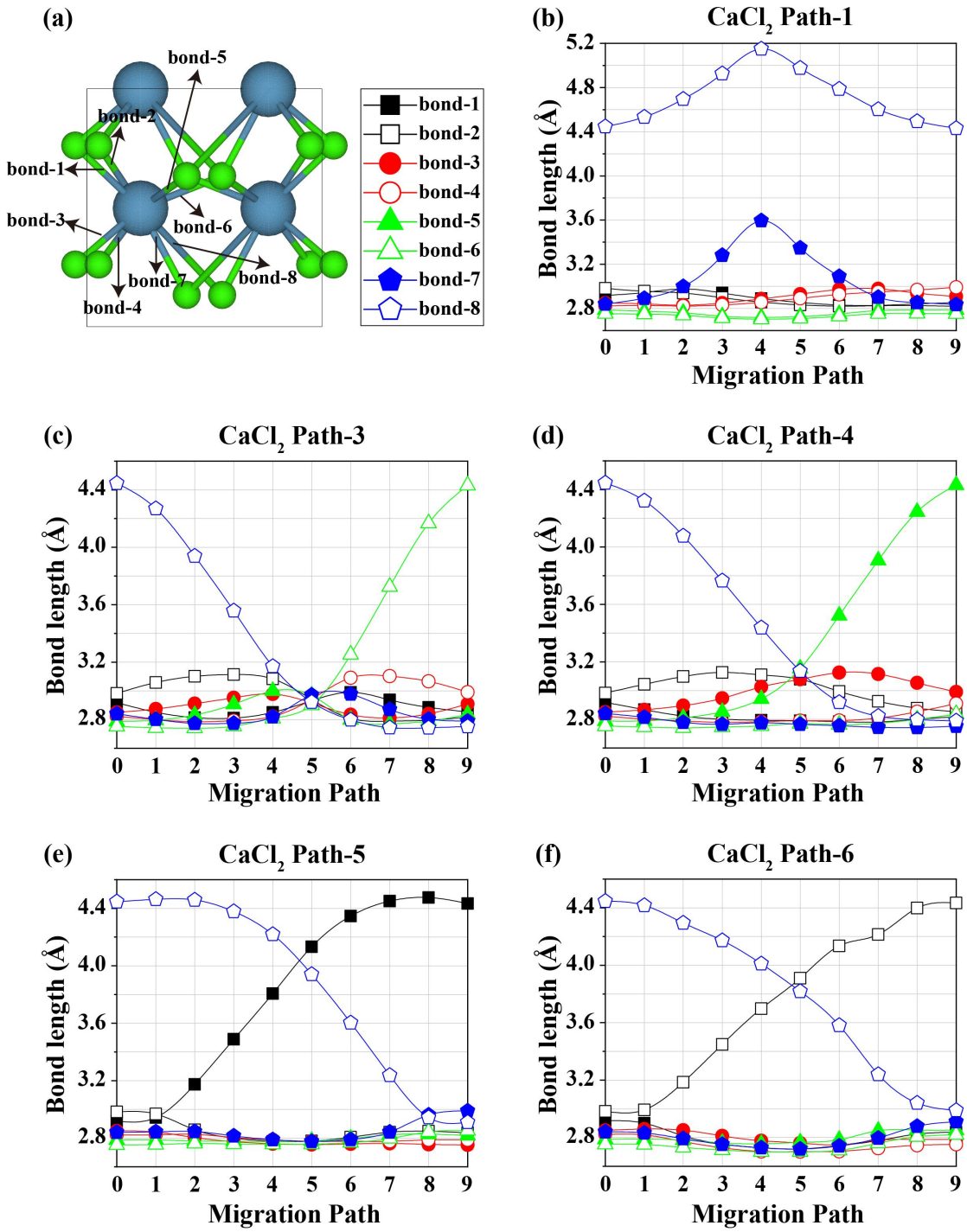

Figure S3. Graphs of bond length variations along the five polarization switching pathways in $CaCl_2$.

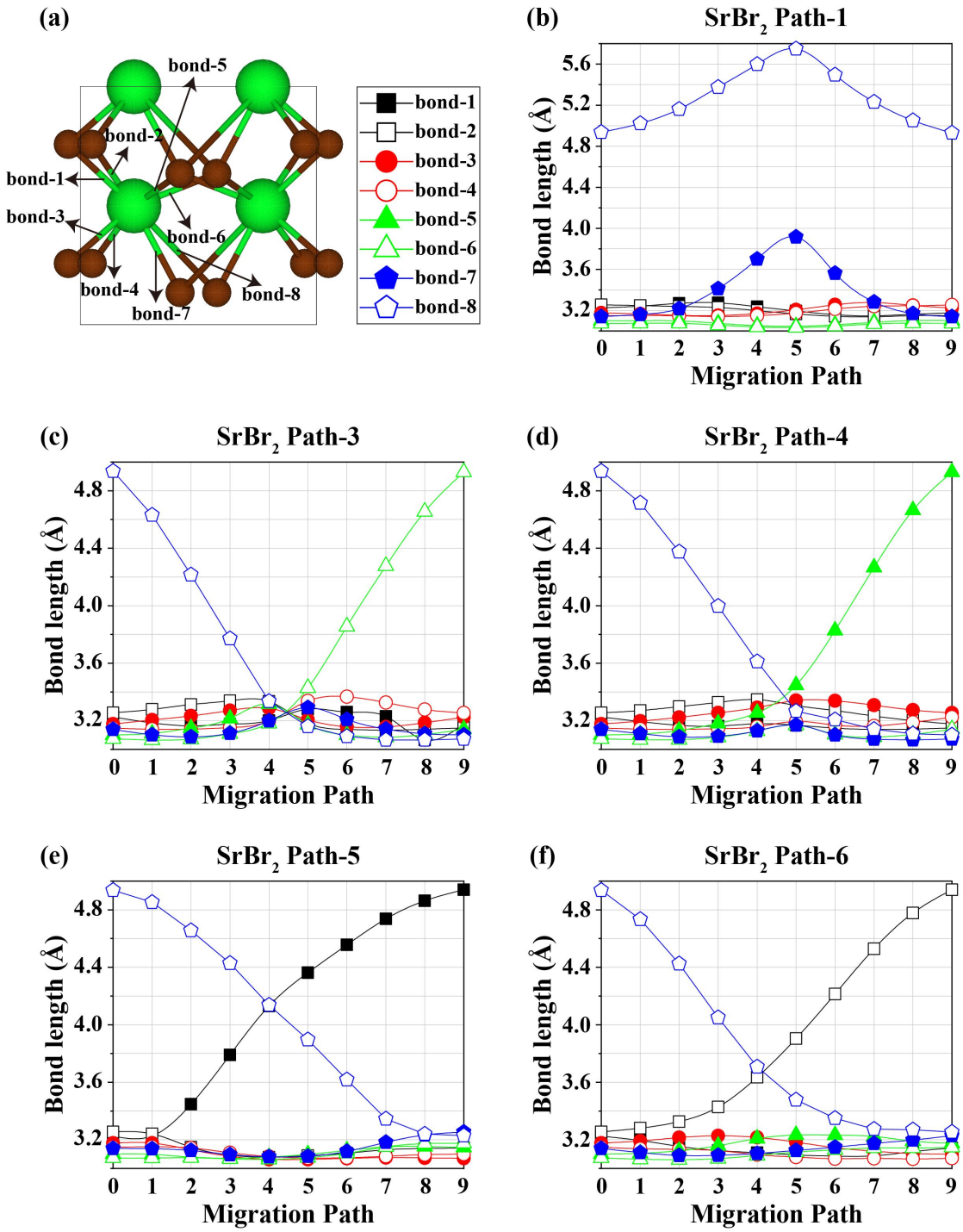

Figure S4. Graphs of bond length variations along the five polarization switching pathways in $SrBr_2$.

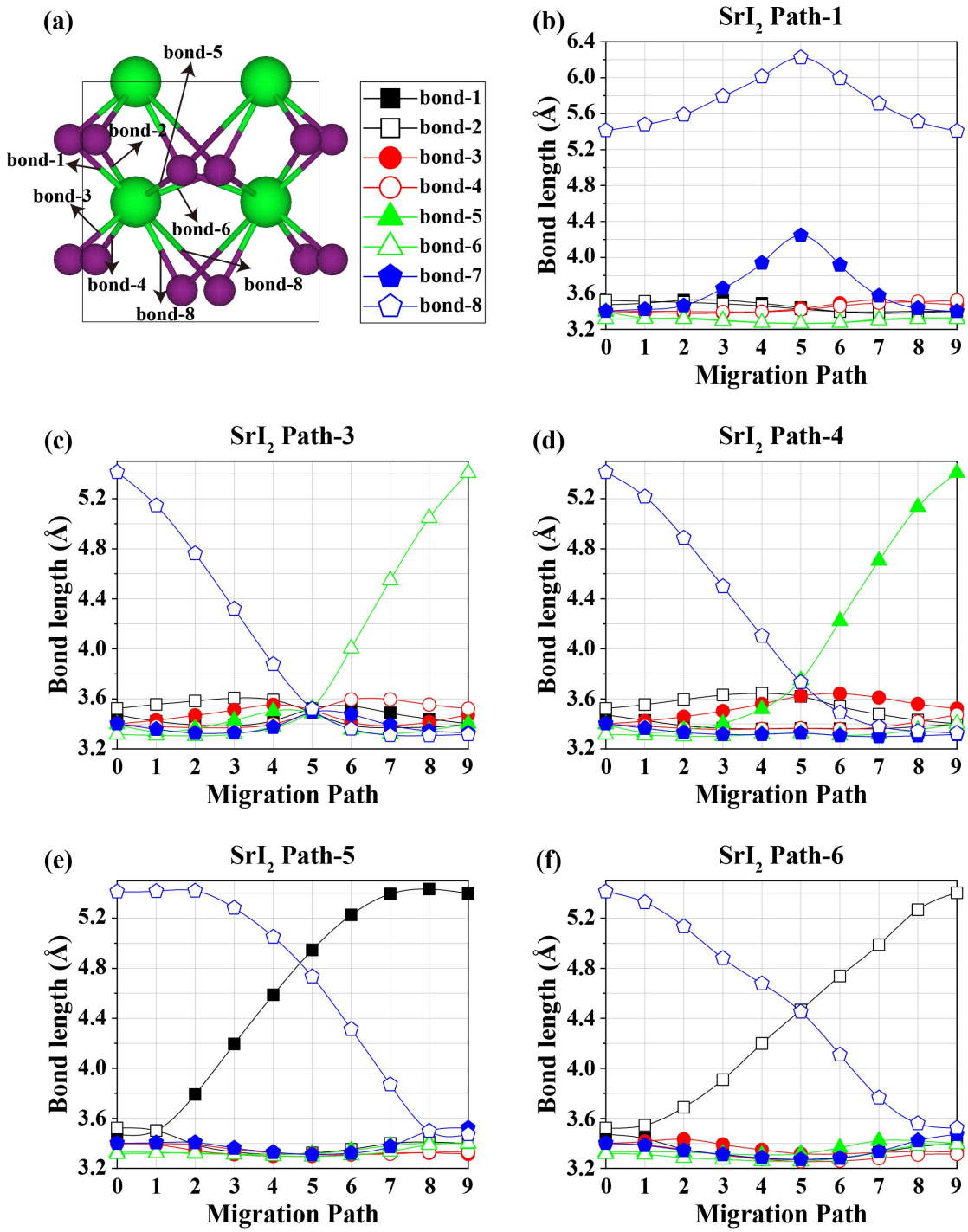

Figure S5. Graphs of bond length variations along the five polarization switching pathways in SrI_2.

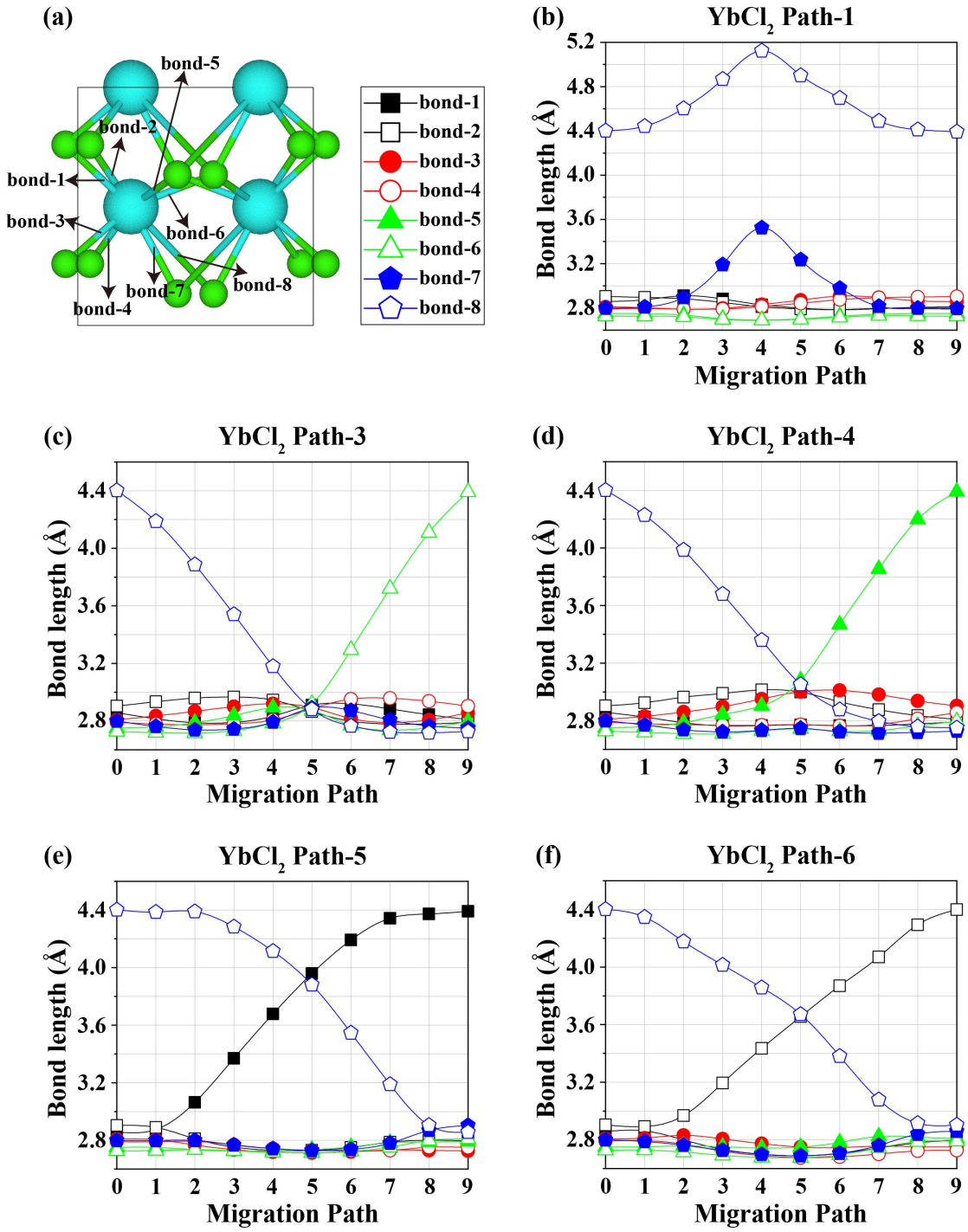

Figure S6. Graphs of bond length variations along the five polarization switching pathways in $YbCl_2$.

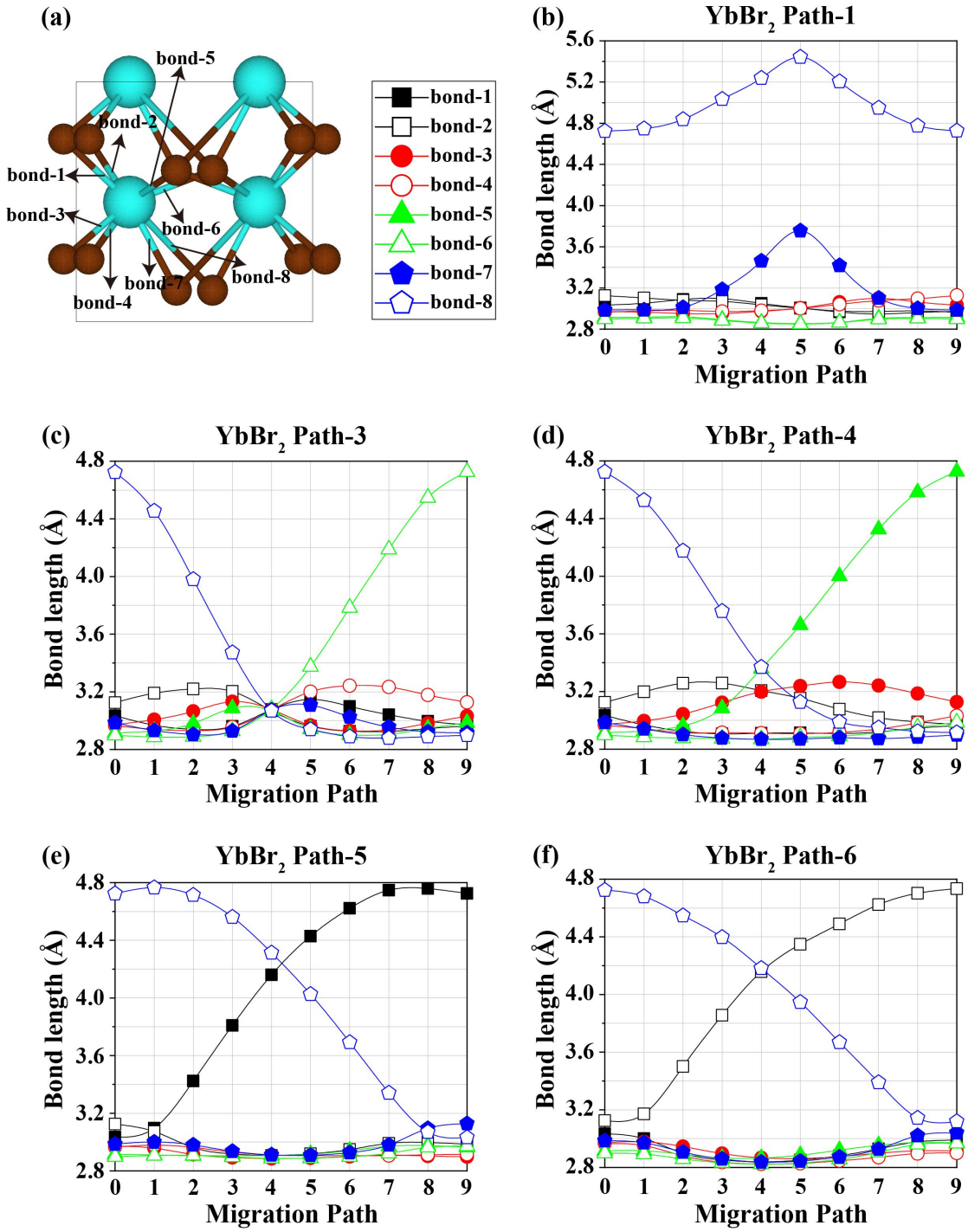

Figure S7. Graphs of bond length variations along the five polarization switching pathways inYbBr$_2$.

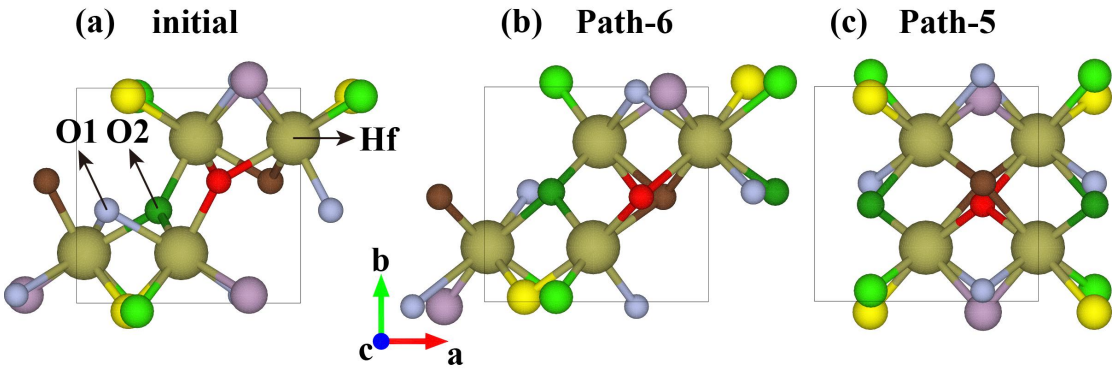

Figure S8. Structures of the ferroelectric phase of HfO_2: (a) initial state, (b) intermediate state along Path-6, (c) intermediate state along Path-5. The four Hf elements (larger spheres) are depicted in the same color, while the other eight atoms (smaller spheres) are all Oxygen atoms and are differentiated by various colors.

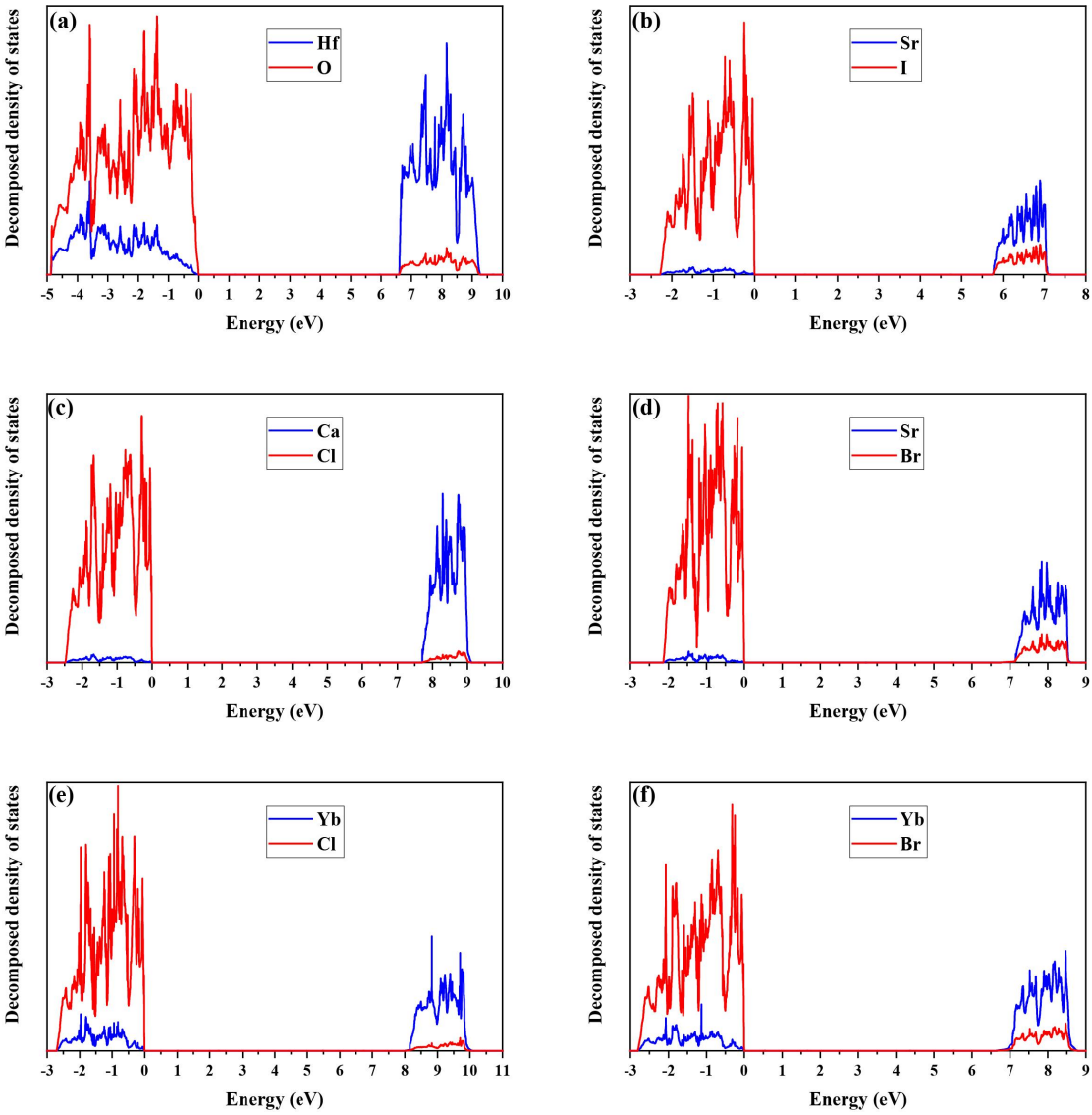

Figure S9. Decomposed density of states of $CaCl_2$, $SrBr_2$, $YbCl_2$, $YbBr_2$ and ZrO_2, calculated using the shell DFT-1/2 method.

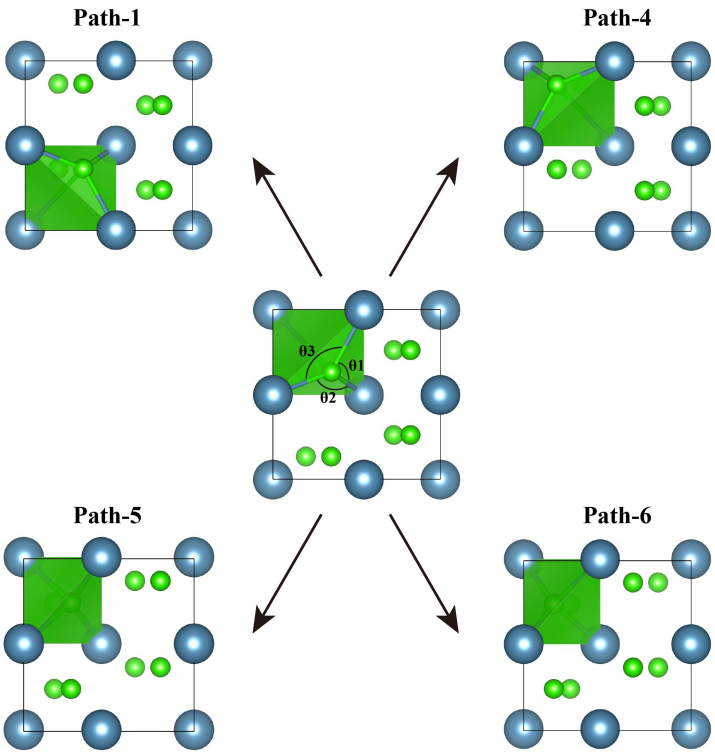

Figure S10： Tetrahedral cage structures of $CaCl_2$, showing the initial structure and final structures for Path-1, Path-4, Path-5 and Path-6 as switching paths.

The positions of O_{III} anions in $CaCl_2$, SrI_2, $SrBr_2$, $YbCl_2$ and $YbBr_2$ are very similar as in HfO_2. As showing in **Figure S10**, taking $CaCl_2$ as an example, O_{III} anions in $CaCl_2$ appear at the surfaces of specific tetrahedra. A simple proof is given here, if the sum of θ_1, θ_2 and θ_3 (**Figure S10**) adds up to 180°, it is proved that the O_{III} is on the plane. The sum of the angles are 359.638°, 359.012°, 358.336°, 358.863°, 358.840° and 358.775° for HfO_2, $CaCl_2$, SrI_2, $SrBr_2$, $YbCl_2$ and $YbBr_2$, which are very close to 360°.

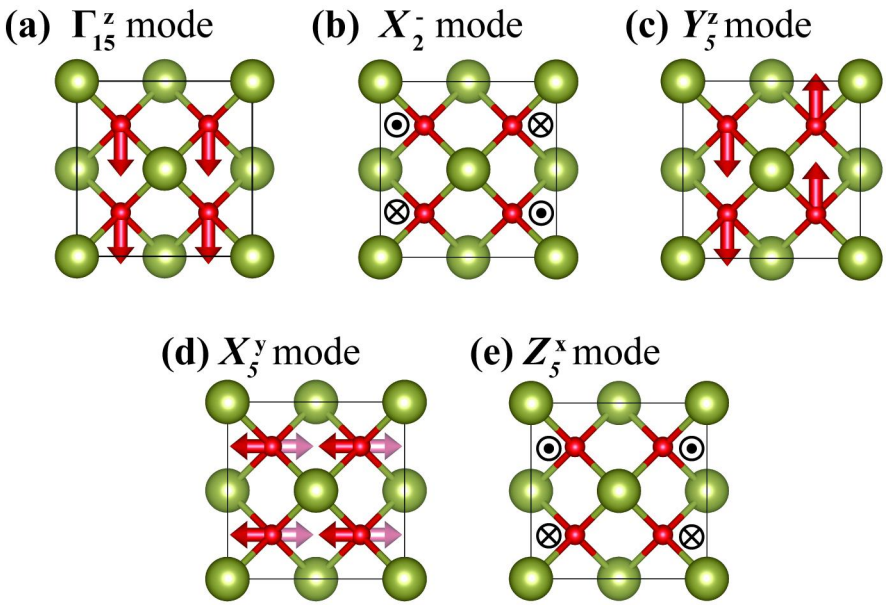

Figure S11： Diagrams of oxygen displacements in five different phonon modes Γ_{15}^{z}, X_{2}^{-}, Y_{5}^{z}, X_{5}^{y} and Z_{5}^{x}.